THE AMERICAN SOCIETY OF MECHANICAL ENGINEERS
345 E. 47th St., New York, N.Y. 10017

UNSTEADY 3D FLOW IN A SINGLE-STAGE TRANSONIC FAN. PART II: UNSTEADY STATOR EXIT FLOW FIELD

M A Cherrett, J D Bryce, and R B Ginder
Defence Research Agency,
Pyestock, Farnborough, United Kingdom

ABSTRACT

Detailed unsteady aerodynamic measurements have been taken in a single-stage transonic fan with a very high stage-hub loading. 2D dynamic yawmeter probes, capable of measuring mean levels and fluctuations in stagnation pressure, static pressure and yaw angle have been traversed at rotor exit and downstream of the stator, along with several types of pneumatic 3D probe. Part I* describes measurements taken at rotor exit. This paper, Part II, describes measurements taken at stator exit when the fan was operating at near peak efficiency, on the design speed characteristic. The measurements indicate the effects of rotor-stator interaction on the development of the viscous endwall-corner flows at the hub and casing. In addition, they illustrate that significant changes in stagnation pressure level occur within much of the stator exit flow field during the rotor passing cycle.

INTRODUCTION

The endwall regions of turbomachinery blade rows are dominated by complex 3D viscous flows which are not modelled well by most current design and analysis methods. However, a large proportion of the loss generated in the compressor is associated with these structures. Bryce *et al* (1993) have shown that the stator endwall regions of the C148 fan, particularly at the hub, are dominated by 3D corner stalls. The aim of the work reported in this paper (Part II) was to study the severity and extent of these flow features and how they vary during the rotor passing period, to elucidate the effects of blade row interaction on their development. Poensgen & Gallus (1991) have shown that flow field unsteadiness has a significant effect on the development of endwall corner stall. However, the cited work was carried out in a low-speed annular cascade with the rotor wakes simulated by cylindrical bars. There have been no measurements reported for a high-speed engine relevant compressor such as C148.

This paper presents data gathered downstream of the C148 stator, where it was possible to take more complete measurements than at rotor exit, see Part I. That is, the stator exit measurements were taken on a 2D area traverse grid; whereas the rotor exit measurements had been limited to a traverse in the radial direction only. In addition, interference between the dynamic yawmeter probe and the adjacent stator had restricted the rotor exit measurements to stagnation pressure only. These problems were not present at stator exit, and therefore the full measurement potential of the dynamic yawmeters could be utilized to yield transient stagnation pressure, static pressure, and tangential flow angle data.

TIME-AVERAGED MEASUREMENTS

The stator exit measurements were taken at 36% of axial chord downstream of the trailing edge, on a grid of 10 radial by 19 equi-spaced circumferential positions covering 1.3 stator pitches. These positions are shown in Fig 1 along with an indication of yawmeter size at mid-span. C148 employed 25 rotor blades and 52 stator blades; the stator exit measurements were taken immediately behind stator #12, while the rotor exit/stator inlet measurements reported in part I, were taken in front of stator #18. Stator numbering started arbitrarily at the starboard casing split-line, with stator #12 being near top-dead-centre. Fig 1 also shows the circumferential distribution of time-averaged random stagnation pressure unsteadiness at mid-span (ie. excluding the periodic unsteadiness due to rotor-passing) expressed as a percentage of local stagnation pressure. This shows that the wake width is approximately 30% of stator pitch at this position.

The yawmeters were used in conjunction with a system developed at DRA to compensate for semiconductor pressure transducer temperature sensitivity. This allowed the transducers

* A description of the C148 transonic fan is found in part I, along with the instrumentation used to take the measurements. The list of the references given in Part I is common to both parts of the paper.

Presented at the International Gas Turbine and Aeroengine Congress and Exposition
The Hague, Netherlands – June 13–16, 1994
This paper has been accepted for publication in the Transactions of the ASME
Discussion of it will be accepted at ASME Headquarters until September 30, 1994

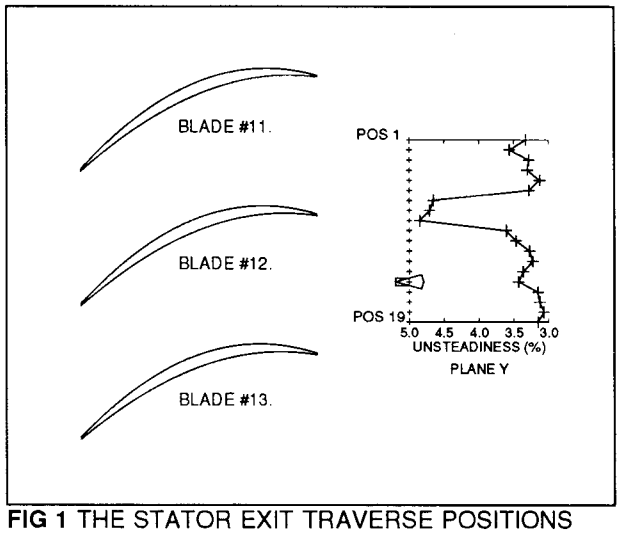

FIG 1 THE STATOR EXIT TRAVERSE POSITIONS AND THE MID-SPAN RANDOM UNSTEADINESS DISTRIBUTION

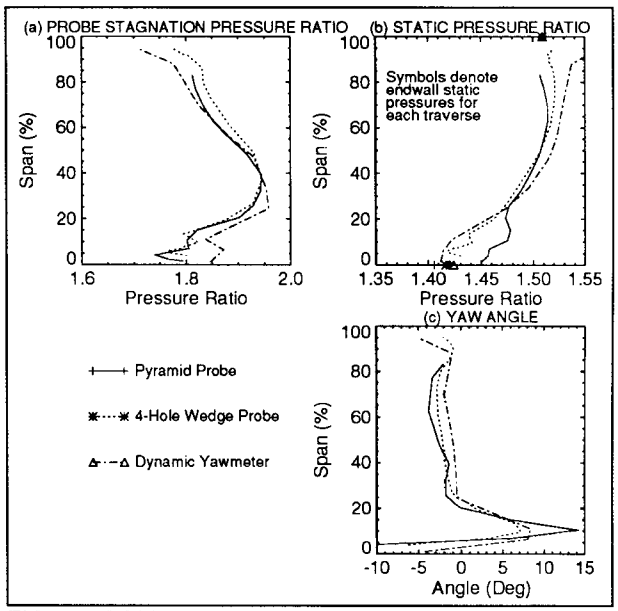

FIG 2 A COMPARISON OF THE YAWMETER MEASUREMENTS WITH THE D PNEUMATIC PROBE DATA

to be used as absolute pressure sensors. However, the effectiveness of this system was compromised by long term temporal drift in the transducer characteristics, ie. over time periods much longer than the time needed to take the yawmeter traverse measurements (see Part I). Even so, with regular calibration it was possible to obtain time-averaged yawmeter measurements that were in good quantitative agreement with pneumatic probe measurements (see below).

Pitchwise averaged results

Fig 2 shows the pitch-wise averaged time-mean pressure and angle measurements taken with the yawmeter, as well as those taken with two 3D pneumatic probes, ie. a 4-hole wedge probe and a sting mounted 4-hole pyramid. Both 3D probes have been illustrated by Bryce *et al* (1993) and discussed more fully by Cherrett *et al* (1992). The stagnation pressure measurements taken with the three probes agree typically to within ±1.0% of the design pressure rise. Static pressure measurements agree to within ±3.0% of dynamic head around mid-span, while yaw angle measurements agree to within 1.0-1.5° over much of the span. Such agreement gives confidence in the yawmeter measurements and implies that, with careful calibration and compensation, the yawmeters are capable of producing time-averaged measurements that compare favourably with pneumatic measurements. However, pneumatic measurement are themselves subject to uncertainty, not least because of the inability of such systems to resolve the fluctuating flows in turbomachinery adequately. Indeed, although the dynamic yawmeters provide an enormous amount of information not obtainable with pneumatic probes, one of the aims cited for their development was to produce probes capable of measuring turbomachinery flows more accurately than pneumatic instruments. Clearly the current levels of transducer temporal instability, discussed in Part I, preclude such performance.

Full traverse results

Figs 3,4 and 5 give more insight into the stator exit flow field by showing the complete time-averaged stagnation pressure, random unsteadiness, and yaw angle (ie. tangential flow angle) data respectively. Each figure also illustrates the pitch-wise variation of the data at 13%, 50% and 90% span, (these positions and the other traverse stations are marked along the edges of the contour plots). In addition, to indicate the time-variance of the results, the maximum and minimum levels occurring in the ensemble-averaged data over the sampled period (equivalent to 22 rotor passages) are shown, together with the rms variation for total pressure and angle. Note that, for the latter quantities, even larger max/min envelopes would be seen if the instantaneous raw data were considered.

The stagnation pressure measurements (Fig 3) clearly illustrate the blade #12 wake, as well as the associated casing and hub corner stalls. The hub-corner stall to the left of the measurements originates from blade #13, and it is more vigorous than that of blade #12. Between the hub-corner stalls there is a region of high stagnation pressure passing through the reduced passage area. This arises from a hub pressure excess at rotor exit, see Part I. Surprisingly, the RMS and max-min pressure variations are similar at the hub and mid-span, but larger toward the casing.

The random unsteadiness data (Fig 4) show considerable activity toward the hub, particularly in the regions between the corner stalls and the high pressure region. This is because of the high unsteadiness in the vigorous shear layer between the viscous and inviscid flow regions, as well as the variation of stall cell size with time (which is discussed below). The yaw angle measurements (Fig 5) generally show steepest gradients and

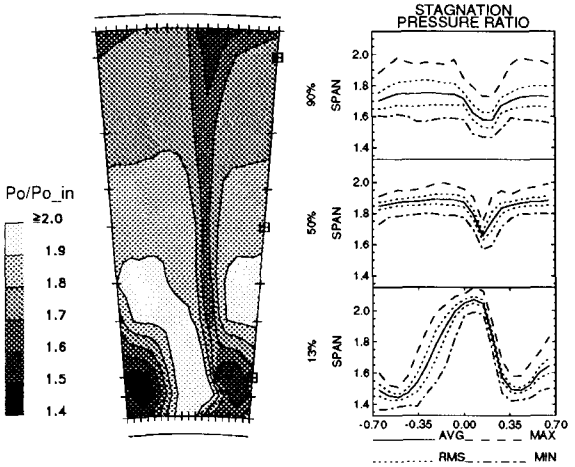

FIG 3 TIME-AVERAGED STAGNATION PRESSURE RATIO MEASUREMENTS

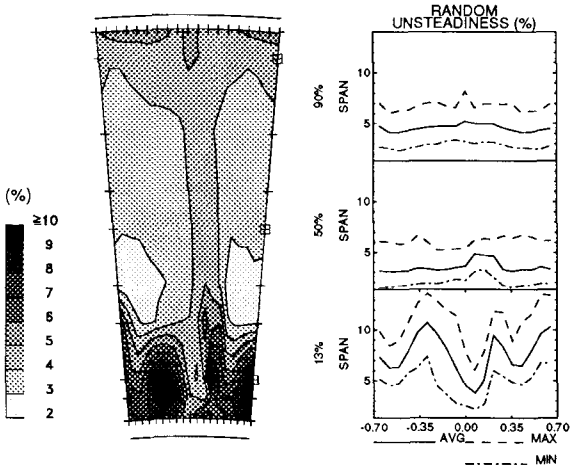

FIG 4 TIME-AVERAGED RANDOM UNSTEADINESS MEASUREMENTS

greatest variations in the viscous end wall and wake flows, and they also display high rms and max-min variations in the casing region. Note that positive yaw is in the direction of rotor rotation which is from left to right in Figs 4,5 and 6.

UNSTEADY MEASUREMENTS

As the yawmeter measurements were taken on a 2D grid downstream of the stator, they may be viewed from several perspectives. Firstly, attention can be focused on a single location and the temporal variation examined. Secondly, the variation of the data across the passage can be viewed at each instant in time and finally, this perspective may be extended to a view of the whole measurement area at each instant in time. It is useful to look at the data from all of these perspectives.

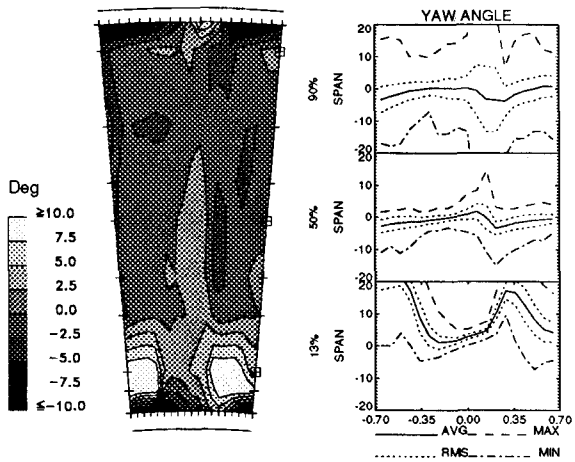

FIG 5 TIME-AVERAGED YAW ANGLE MEASUREMENTS

Single point results

In Fig 6, the data are viewed from the first perspective, focusing on measurements in the stator mid-passage at mid-span (ie. traverse position 15 in Fig 1). The temporal variation of random unsteadiness, ensemble-averaged stagnation pressure, and yaw angle are shown at stator inlet and exit (ie. planes X & Y in Fig 1 of Part I). The inlet measurements were taken close to the stator leading edge and no yaw angle data are available here for reasons explained in Part I. At stator inlet, the rotor wakes are clearly identifiable by high levels of unsteadiness and occupy approximately 30% of the rotor passing period. By plane Y, the unsteadiness level has approximately halved and the rotor wakes broadened to occupy approximately 75% of the passing period.

The ensemble-averaged pressure measurements at inlet are dominated by perturbations at two and three times blade passing frequency, as discussed at length in part I. The stator exit measurements are of similar complexity, but the amplitude of the oscillations at mid passage (position 15) in plane Y are less than those at inlet, although this is not true of all the pitch-wise positions in plane Y at mid-span. It will be shown in the forthcoming discussion that the amplitude and frequency of the pressure oscillations at stator exit are connected with the expansion and contraction of the high pressure region toward the hub.

The yaw angle variations at stator exit in Fig 6 show that these are as complex as the stagnation pressure results. Relating the yaw angle data to the random unsteadiness variations, it is apparent that the flow momentarily undergoes a negative perturbation (ie. against the direction of rotor rotation) on the pressure side of the rotor wake; followed by a positive angle perturbation on the suction surface side of the rotor wake. It would be expected that 'negative jet' effects within the chopped wakes convect fluid from the suction to pressure surface sides of the passage, ie. giving rise to a positive angle perturbation near the wake centre. However, the strongest angle perturbations in Fig 6 are in the opposite direction on the windward (pressure

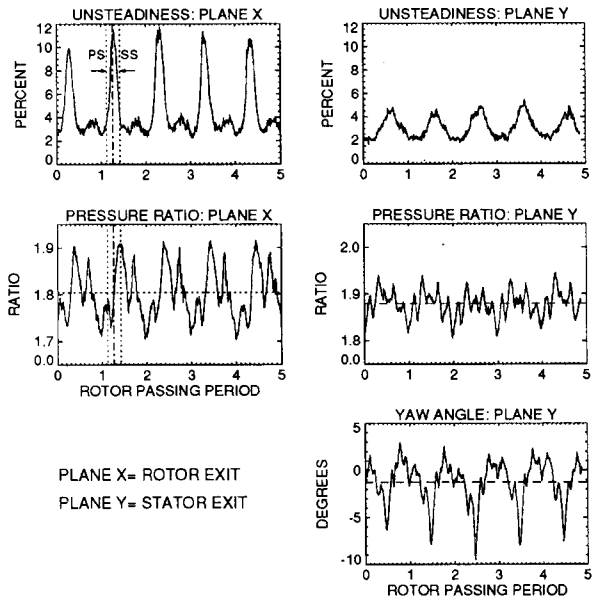

FIG 6 UNSTEADY FLOW FIELD MEASUREMENTS AT STATOR INLET AND EXIT

surface) side of the wake. The measured behaviour may indicate the presence of counter rotating vortices set up on either side of the chopped wakes as they pass through the stator passage. However, without measurements on the blade-to-blade plane it is difficult to explain fully the yaw angle behaviour in Fig 6.

Area traverse results

A more comprehensive view of the stator exit flow field measurements is shown in Fig 7. (In the interests of brevity, the following discussion is restricted to the consideration of ensemble averaged stagnation pressure ratio and random unsteadiness.) Fig 7 contains several perspectives of the stator exit measurements 'frozen' at the same instant in time within the rotor revolution, but derived by averaging over 128 consecutive rotor revolutions. These perspectives are described below.

a) This is a view of the instantaneous random stagnation pressure unsteadiness field expressed as percentage of local time-averaged stagnation pressure using the same grey-scale as Fig 4.

b) This is a view of the instantaneous ensemble averaged stagnation pressure ratio. In this, as in a), the stator passage is viewed from the rear looking upstream and the upstream rotor rotates clockwise. The grey scale is the same as that used in Fig 3.

c),d) These images show the temporal variation of ensemble-averaged stagnation pressure ratio at two positions in the mid-span traverse. One point is situated on the suction surface side of the stator passage (position 18 in Fig 1), and the other on the pressure surface side (position 11). The time ordinate in these images is expressed as a fraction of blade passing period and the instant at which time is frozen in Fig 7 is illustrated by the * symbols superimposed on the time-histories in c) & d).

e) This shows the instantaneous distribution of random stagnation pressure unsteadiness across the stator passage at mid-span. The instantaneous distribution is plotted as a solid line, while the time averaged data are plotted as + symbols.

f) This is similar to e), but illustrates the variation of ensemble-averaged stagnation pressure ratio across the stator passage at mid-span.

g) A 'clock' indicating the fraction of rotor passing period at which the images in Fig 7 have been frozen in time.

In Fig 7a, a rotor wake (labelled i) lies diagonally across the passage to the left of the stator wake. At mid-span, see Fig 7e, there is a localized region where the unsteadiness levels in the rotor wake approach those in the stator wake, although elsewhere the rotor wake unsteadiness levels are lower than in the stator wake. Wake i, in Fig 7a, also appears in the passage to the right of the stator wake. It was possible to confirm that this, and the disturbance identified in the left hand passage are parts of the same chopped wake because some rotor wakes were notably weaker than others. This allowed them to be identified easily (although this is not illustrated specifically in this paper). The previous rotor wake (i-1) is also visible in the right hand stator passage as it leaves the traversed area.

Fig 7 is part of a data set that documents a little over 22 rotor passing periods, with 92 measurements being taken within each passing period (ie. 2048 sets of images in total). Because of the volume and complexity of the data, computer based data animation was employed extensively to analyze the measurements and it is difficult to imagine how the data could be analyzed effectively in any other manner. However, using these techniques it was possible to animate only a small portion of the data at a time, with one or more rotor passing periods being spliced from the main data set and animated cyclically. It was found that at least 30 images per rotor passing period were necessary to construct a sequence that resolved the rotor passing period effectively. Clearly it is not practical to present such a large volume of data here, and hence 8 images from a typical blade passing cycle are presented in Fig 8 to illustrate the effects of rotor passing on the stator exit flow field. It should be noted that these images are not evenly spaced in time about the rotor blade passing period.

In Fig 8, the data are arranged in chronological sequence starting at the top left hand corner of the figure and preceding in a clockwise manner as indicated by the ascending Roman numerals. Rotor rotation is in the same direction, and the first image (Fig 8_I) shows the same data as Fig 7. Because of the complexity of the data in Fig 8, the reader is advised to take a macroscopic view of the data making reference to the observations highlighted below before attempting a more detailed interpretation. The relative coarseness of the traverse grid, particularly in the radial direction, should be borne in mind. Also, Part I of this paper should be consulted to become acquainted with the structure of rotor exit flow field, particularly near the endwalls. It should also be noted that the ensemble-averaged stagnation pressure measurements presented in Part I

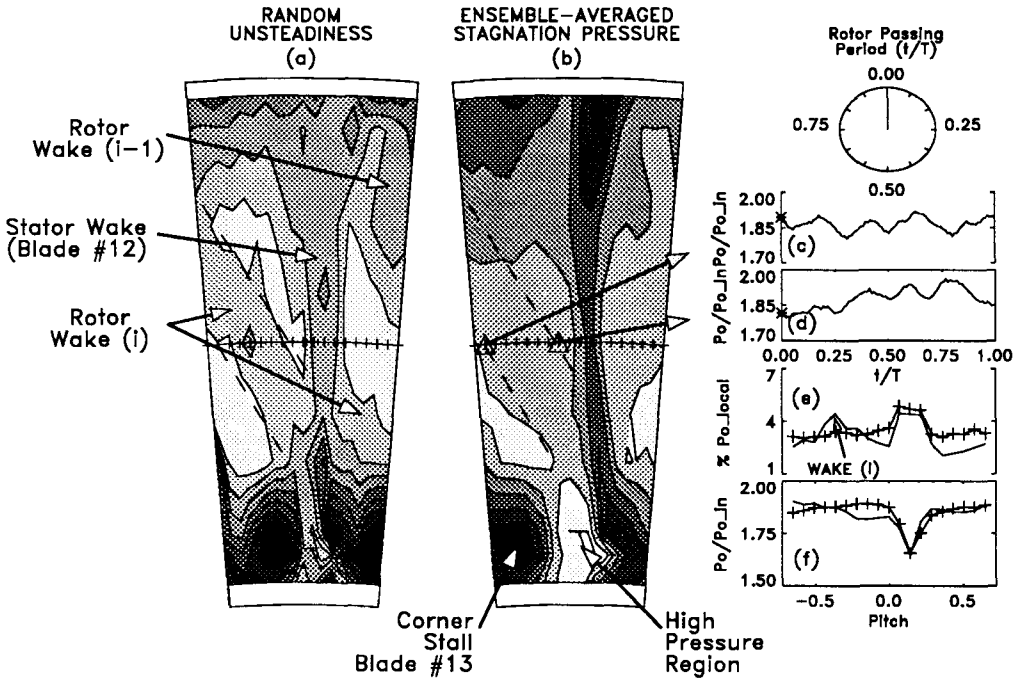

FIG 7 INSTANTANEOUS UNSTEADINESS AND PRESSURE RATIO MEASUREMENTS (GREY SCALES ARE THE SAME AS IN FIGS 3 & 4)

were ac-coupled, whereas those in Figs 7 & 8 document both ac and dc-pressure components.

Behaviour of the hub-corner stalls The rotor wakes are clearly visible in the random unsteadiness measurements (ie. the equivalent images to Fig 7a), and these data are most useful for tracking the rotor wake positions. However, insight into the effects of rotor passing is best gained through examination of the stagnation pressure ratio measurements, particularly in the left hand passage between stators #12 & #13 as most of this is visible in the images equivalent to Fig 7b.

Consideration of the left hand stator #13 hub-corner stall reveals that it is at its largest, and contains the lowest pressure levels, in Figs 8_{I} & 8_{II}. The same stall is smallest approximately half a period later, in Figs 8_{IV} & 8_{V}. The right hand stall behaves in a similar manner, but is 180° out of phase. This is consistent with the effects of rotor passing because there are approximately two stator blades for each rotor blade (ie. 52 vs 25). During the rotor passing period, pressure ratio variations within the centre of the hub stalls are some ±5% of the local time-averaged values, which is comparable with the maximum-to-minimum variation found throughout most of the entire plane Y pressure field. However, because the size of the stalls wax and wane, pressure levels at the boundary of the stalls and the inviscid core flow vary by ±10-14%. These fluctuations are found within the ensemble-averaged measurements, and even higher levels would occur within the instantaneous pressure time histories from which these data are derived. However, while it is certainly responsive to rotor passing, the stator hub stall would appear to be a fundamentally steady-state phenomenon predictable (in principle) by steady-state 3D viscous calculations.

Relating the hub-stall size to the rotor wake positions, it is evident that they are at their largest after the rotor wake has passed the stall, and that this swollen state persists for some time afterwards. For instance, the hub-end of rotor wake i+1 passes the blade #13 stall between Figs 8_{V} & 8_{VI}, yet the stall becomes and remains enlarged during sequence between Figs 8_{VII} to 8_{II}. It is suspected that this is due to the rotor hub corner stall (see Part I) that extends in a pitch-wise direction across the endwall for some 60% of the rotor pitch, or passing period. It is thought that the rapid increases in random pressure unsteadiness and large changes in pressure and incidence that accompany this region induce a growth in stator hub stall.

It should also be noted that the rotor potential field is expected to have a significant effect on the stator hub flow field. This is clear in Fig 1 in part I, which shows the thick rotor root section juxtaposed to the slender stator hub sections. Of course, in assessing the magnitude of potential interaction the gross distortion of the effective blade shapes by the local 3D viscous flows needs to be taken into account. Therefore, although there are a number of CFD codes that provide useful insights into the

magnitude of potential interaction, these are of little practical use where both blade rows are dominated by 3D viscous flows.

Behaviour of the inviscid high pressure region Perhaps the most striking feature in the data in Fig 8 is the behaviour of the inviscid high-pressure region in the lower half of the annulus between blades #12 & #13. As mentioned earlier, this feature has its origin in the pressure excess noted at rotor exit in Part I but it is subsequently affected strongly by blade row interaction. In Fig 8_{I} this region is at its smallest where it is constrained between the blade #13 stall (which is at its zenith), the pressure surface of the blade #12 wake, and leeward side of rotor wake i. As rotor wake i moves away, the stator passage becomes progressively more free of its influence, the blade #13 stall begins to subside, and the high pressure region begins to expand radially. The expansion becomes more vigorous in Fig 8_{IV} as rotor wake (i+1) enters the passage, and the high pressure region reaches its greatest extent during Fig 8_{V}, after which it begins to contract.

This ordered cycle of expansion and contraction during the rotor passing appears to be contradicted in Fig 8_{VII}, when a high pressure region grows suddenly near the pressure surface side of the stator #12 wake near mid-span. The video animation, from which these images were extracted, shows that this high pressure region grows very suddenly from the otherwise low pressures found on the advancing side of the rotor wake and dissipates as quickly. As such it may not be linked directly to the high pressure region between the hub corner stalls.

It should also be noted that the expansion and contraction of the high pressure regions does not necessarily imply that the fluid is subjected to strong radial transportation. Rather, much of the observed behaviour is probably be due to the fact that the rotor wake (and potential) flows are skewed circumferentially relative to the almost radially aligned stators. Therefore, the stator hub is influenced first by the rotor flow, and subsequent blade row interactions occur later at increasing blade heights.

While it is possible to make an objective assessment of the behaviour of these features, it is far more difficult to explain the blade row interaction mechanisms causing the behaviour. Indeed it is not clear how complete an understanding can be achieved using data taken in only one stator exit traverse plane. However, it is hoped that continued analysis, relating the stator inlet and exit flows, as well as the on-blade measurements taken throughout the passage at mid-span, will shed more light on the behaviour.

Rotor wake Closer examination of the rotor wake as it crosses the stator passage reveals that it becomes discontinuous either side of the stator wake. This is to be expected, as the rotor wake is predicted to travel faster on the suction surface of the stator blade than on the pressure surface. This is more noticeable as the chopped rotor wakes progress up the stator wake and the difference between the arrival times of the wake segments either side of the stator wake becomes more significant, ie. compare Figs 8_{III} & 8_{IV}.

In Figs 8_{VII} & 8_{VIII} the unsteadiness in wake (i+1) as it leaves the suction surface side of the stator #13 wake near mid-span is higher than that attained elsewhere in the rotor wake. From the video animation this effect is also seen in wake (i) as it leaves the stator #12 wake. Similarly, it is evident that these features persist longer than the passing of the rotor wake alone can account for. It is thought that this is an artefact of localized suction surface boundary layer separation induced by the passing rotor wakes. However, it is notable that this behaviour seems to be prevalent near mid-span only.

Behaviour of the casing-corner stalls Discussion so far has concentrated on events occurring in the bottom half of the annulus. However, in Fig 8 it can be seen that there is significant unsteadiness toward the casing and in particular, the blade #12 casing-corner stall varies in size and strength significantly. In addition, the range of maximum-to-minimum ensemble-averaged pressure levels recorded within even the inviscid core flow are ±8-15% of the local time-averaged pressure ratios, which is somewhat larger than elsewhere in the passage. Unfortunately, random unsteadiness levels are also higher in the upper part of the annulus, which makes identification of the rotor wake positions less certain and hampers detailed interpretation of the flow field. Even so, it is clear that the casing stall is enlarged between Figs 8_{VI} and 8_{II}, ie, some 30% of the rotor passing period. The correlation between the this time interval and the spatial extent of the rotor tip leakage flow (shown in Part I) suggests that the casing corner stall is strongly, and adversely, influenced by the passing rotor leakage vortex. This reflects the behaviour of the hub corner stalls, which were adversely affected by the rotor hub end wall flows; and is compatible with work reported by Howard *et al* (1993), which showed (using time-averaged measurements) that rotor tip clearance has a significant influence on loss generation in the subsequent stator casing region.

Intra-passage pressure oscillations The time-history images equivalent to Figs 7c & 7d in Fig 8 are of course local manifestations of the changes in the radial and circumferential extent of the stagnation pressure features measured in the 2D stator exit traverse plane. For example, during the part of the cycle where the hub high pressure region expands and contracts most vigorously (Figs 8_{IV} to 8_{VI}) the asterisks in these time histories negotiate local peaks. While a complete explanation for all of these perturbations is not yet possible, other effects such as the passing of rotor wakes are clearly significant.

DISCUSSION

It is clear that the flow field perturbations measured across the 2D stator exit traverse plane are very complex, and that they cannot be explained fully in terms of the measured rotor exit flow field (discussed in part I) sweeping past the stator row. The reasons for this additional complexity are most likely due to the following factors. i) The rotor exit flow field may change as it sweeps past the downstream stator. This was thought to be the case in Part I, although this could not be confirmed because the measurements at rotor exit were taken at only one circumferential location near the stator leading edge. ii) The stator flow field will be altered as the chopped rotor wakes are convected through the stator passage. iii) The viscous endwall flows have been shown

to alter those in the downstream stator, and this will affect the flow elsewhere in the stator passage.

The complicated co-existence of these blade row interaction effects is thought to be responsible for the pressure oscillations measured at stator exit. Similarly, because of the broadly similar nature of the oscillations at rotor exit it seems reasonable to suppose that they too are due to blade row interaction. It is more difficult to imagine that they are connected with rotor shock oscillation due to vortex shedding as hypothesised by Epstein et al (1988). Additionally, the most vigorous perturbations seem to be linked strongly with phenomena occurring in the lower half of the annulus, where the rotor shock system is weakest. This is not consistent with rotor shock effects being a primary source as these would be strongest at higher radii.

These observations may also apply to the rotor exit pressure oscillations reported by Ng & Epstein (1985), Gertz (1986) and Cherrett & Bryce (1991). In formulating the oscillating shock hypothesis Ng & Epstein (1985) did not have access to such extensive data as presented here and were constrained to seeking an explanation based on a 2D blade-to-blade view of the rotor. However, it is certainly not denied that rotor shock oscillation exists, as full field optical measurements taken elsewhere clearly indicate such behaviour. Rather, this may be driven by more global interactions between rotor and stator flow fields during the blade row interaction cycle. Clearly more work is required to investigate this further.

In viewing the area traverse results there are, in addition to indisputable 3D effects such as interaction between rotor and stator corner stalls and tip vortices, other apparent 3D effects such as the radial growth and decay of the high pressure region toward the hub. Whether the latter effects are really 3D, or can be largely explained on a 2D blade-to-blade basis (with apparent spanwise propagation occurring due to changes in phase along the blade span) is not yet clear. Flow calculations using unsteady viscous blade-to-blade methods may throw further light on the problem and these are being pursued.

In general further analysis of existing data taken using on-blade pressure sensors and thin-film gauges and relating them to the stator inlet and exit flow field measurements will hopefully enhance understanding. Calculations using steady, and ultimately unsteady, 3D flow solvers will contribute, and the C148 measurements of course represent an excellent database for the development of these. In the longer term, more comprehensive unsteady measurements would also be helpful in reaching a better understanding. The use of 3D unsteady probes that can distinguish radial components of the flow and the adoption of 2D area traversing at rotor exit would be particularly beneficial.

The data clearly show the need to take such measurements in high-speed engine relevant machines. The published material that detail the effects of rotor-stator interaction on the endwall flow development in compressor stators, tend to be of the sort reported by Gallus & Schulz and their co-workers. These excellent low-speed experiments have done much to further understanding of the effects of viscous blade wake impingement on downstream stator rows. However, as these studies utilized a rotating bar to simulate the rotor, the resulting behaviour may be somewhat misleading. For instance, it has been shown in the C148 data that the stator endwall flows are strongly influenced by the viscous flow features originating in the upstream rotor endwall regions.

CONCLUSIONS

Detailed measurements have been taken with a dynamic yawmeter traverse probe downstream of a highly loaded transonic fan stator row. Using a method to counter the temperature sensitivity of the high-frequency response pressure transducers used in the probes, it was possible to obtain absolute pressure measurements from the sensors. Comparison of the yawmeter data with those taken using a variety of pneumatic probes, showed the time-averaged yawmeter results to be in very good agreement with the conventional measurements. The following remarks summarize the analysis carried out to date.

1 The stator hub and casing corner stalls change in size during the rotor passing period. This behaviour appears to be coupled closely to the passing of the viscous endwall features originating in the upstream rotor row.

2 Large changes in stagnation pressure occur within the inviscid stator core flow regions during the rotor passing period.

3 Because 2D area traverse were carried out at stator exit, it was possible to see that the complicated individual pressure time-histories were linked to the expansion and contraction of high pressure zones in the measurement plane. As the stator exit time-histories bore close similarity to those measured at rotor exit in C148 and other high-speed compressors, it is suggested that blade row interactions are responsible for both. However, 2D rotor exit traverses are needed to confirm this.

4 Computer based animation was employed extensively to analyze the stator exit measurements, and it is difficult to imagine how else one could assimilate data of this complexity and volume.

The data presented in this paper and Part I are complex, and there is much more analysis yet to be done. However, it is unlikely that a full explanation of the observed behaviour can be gleaned from the stator exit results done. Further analysis, relating the stator inlet and exit flow fields to measurements taken using on-blade pressure sensors and thin-film gauges will hopefully shed more light on the mechanisms involved. This analysis will also be supported by a range of steady-state and unsteady CFD methods.

ACKNOWLEDGEMENTS

The C148 measurements were supported by the UK MoD Strategic Research Programme and by the Aerospace Division of the UK DTI. Thanks are due to Iain Shipman for his help in putting the paper together.

REFERENCES

A complete set of references applicable to Parts I & II of the paper are included in Part I.

FIG 8(I)

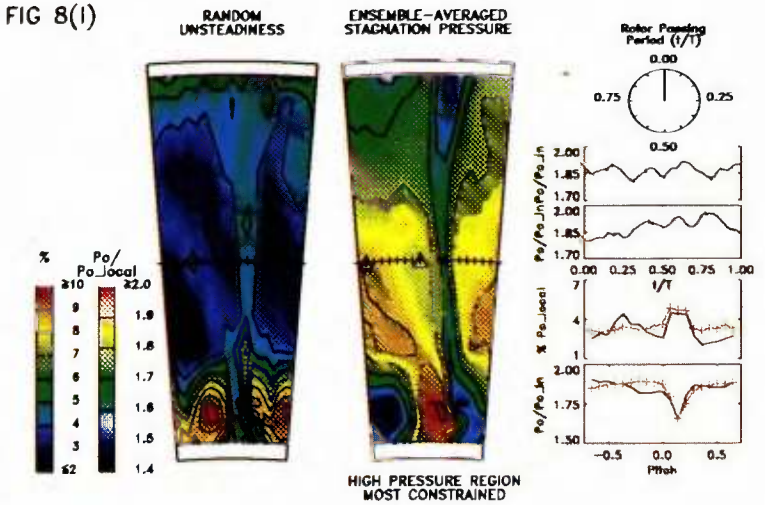

START⇒

FIG 8(VIII)

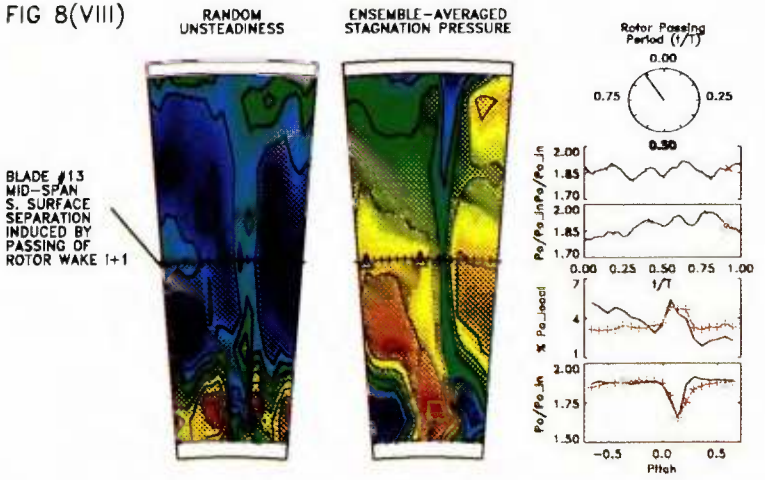

⇑

FIG 8(II)

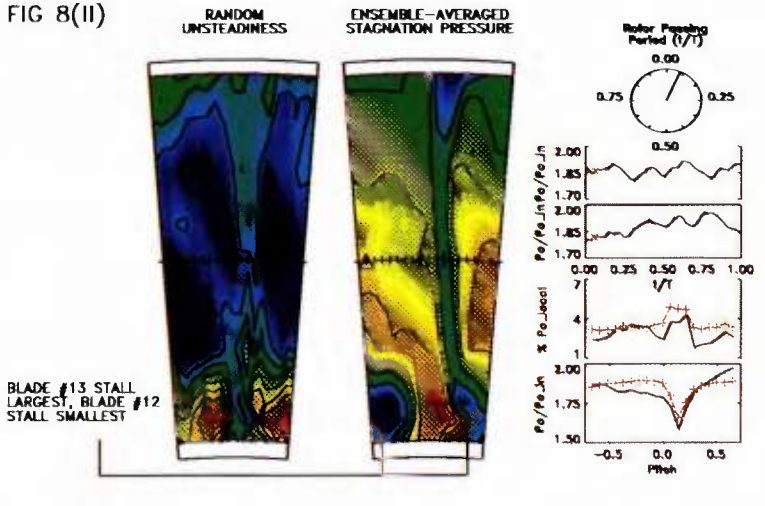

⇓

FIG 8(III)

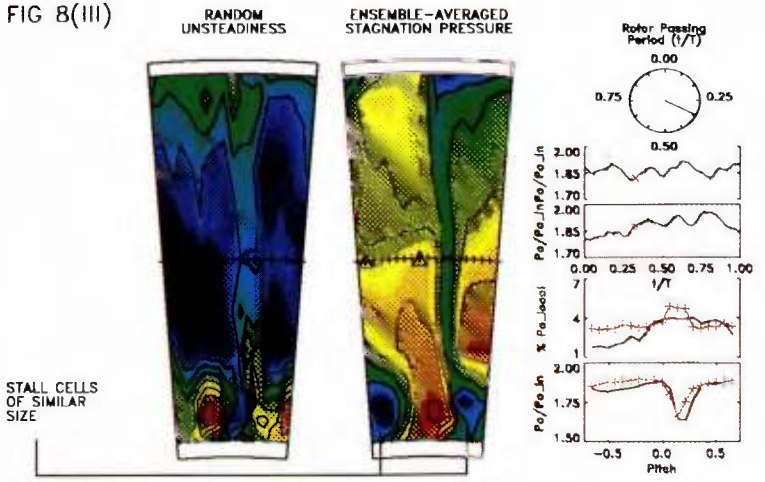

⇓

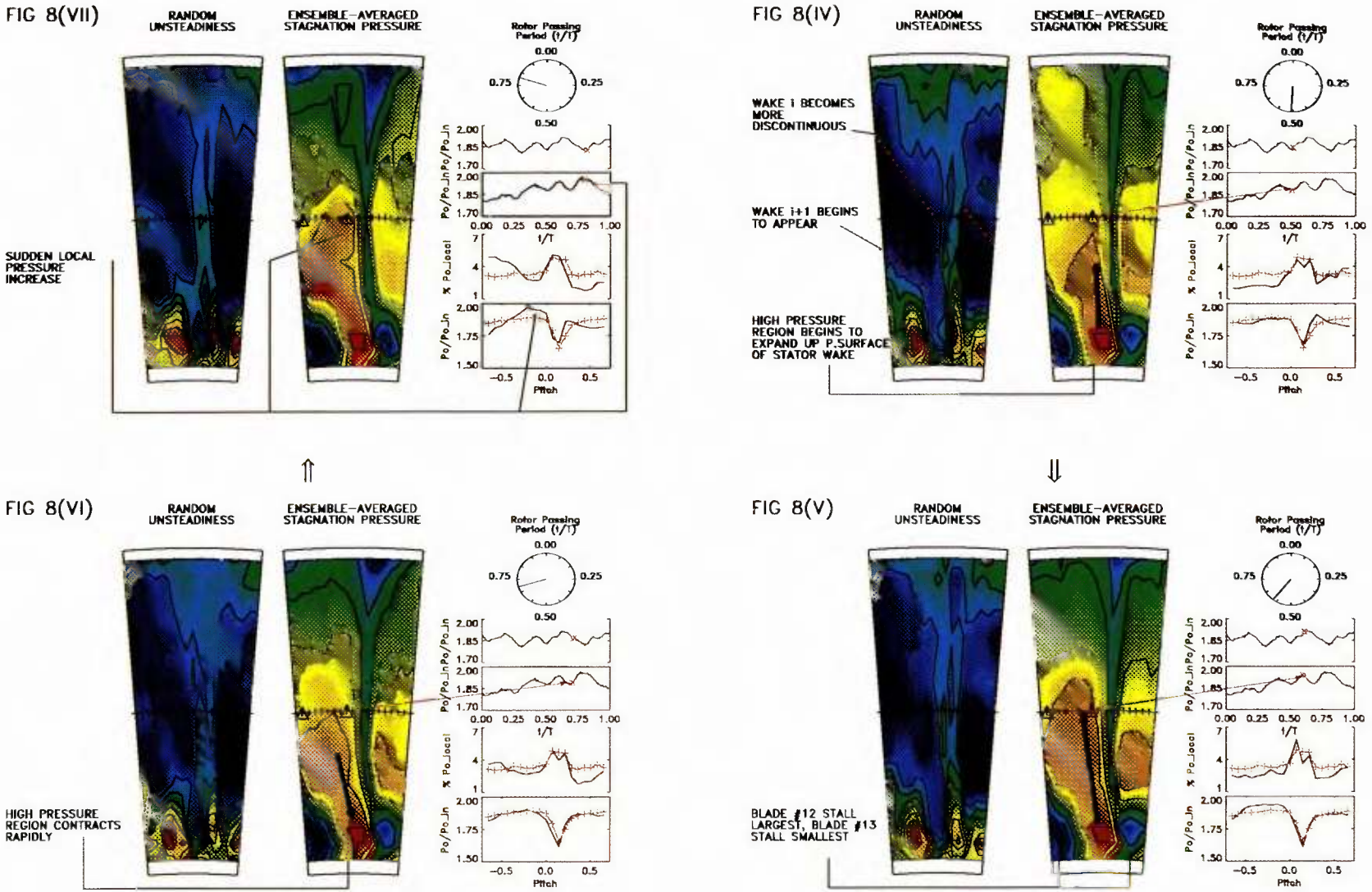

FIG 8 THE EFFECTS OF ROTOR PASSING ON THE STATOR EXIT FLOW FIELD